Multiscale analysis of single- and multiple-pulse laser-induced damages in HfO_2/SiO_2 multilayer dielectric films at 532 nm

Wenwen Liu (刘文文)[1,2], Chaoyang Wei (魏朝阳)[1,*], Kui Yi (易 葵)[1], and Jianda Shao (邵建达)[1]

[1]*Key Laboratory of Materials for High Power Laser, Shanghai Institute of Optics and Fine Mechanics, Chinese Academy of Sciences, Shanghai 201800, China*

[2]*Graduate School of Chinese Academy of Sciences, Beijing 100039, China*

**Corresponding author: siomwei@siom.ac.cn*

Received April 24, 2015; accepted June 30, 2015; posted online August 5, 2015

Nanosecond single- and multiple-pulse laser damage studies on HfO_2/SiO_2 high-reflection (HR) coatings are performed at 532 nm. For single-pulse irradiation, the damage is attributed to the defects and the electric intensity distribution in the multilayer thin films. When the defect density in the irradiated area is high, delamination is observed. Other than the 1064 nm laser damage, the plasma scalding of the 532 nm laser damage is not pits-centered for normal incidence, and the size of the plasma scalding has no relation to the defect density and position, but increases with the laser fluence. For multiple-pulse irradiations, some damage sites show deeper precursors than those from the single-shot irradiation due to the accumulation effects. The cumulative laser-induced damages behave as pits without the presence of plasma scalding, which is unaffected by the laser fluence and shot numbers. The damage morphologies and depth information both confirm the fatigue effect of a HfO_2/SiO_2 HR coating under 532 nm laser irradiation.

OCIS codes: 140.3330, 140.3440, 140.3380.

doi: 10.3788/COL201513.091404.

Dielectric coatings at a wavelength of 532 nm are used in a Ti:sapphire chirped-pulse amplification laser system, which has drawn more and more attention to the fabrication of high quality, 532 nm dielectric coatings. Compared with 1064 and 355 nm optical coatings, there has been relatively little research conducted on 532 nm optical coatings, especially on the multiple pulse laser-induced damages of these coatings[1,2]. However, in practical applications, the optics used in high-power laser systems are always subject to multiple-pulse irradiations. It is well established that the damage threshold of dielectric materials subjected to multi-pulse exposure is sometimes lower than that generated under single-pulse illumination, an effect that is sometimes referred to as the fatigue effect[3–5]. The incubation phenomenon implies laser-induced modifications to the material, which weakens its resistance to subsequent pulse exposure and affects the long-term working stability of the optics. Thus, investigations of single- and multi-pulse laser-induced damages on optical coatings at 532 nm are of high necessity and practical importance for high-power laser applications[6–8].

As we already know, in HfO_2/SiO_2 multilayer coatings at 1064 nm, nodular defects are the most critical defects for single-pulse irradiation, and laser-induced defects or intrinsic defects with irreversible changes are attributed to laser-induced damages under multiple irradiations[9–11]. Since they are different from 1064 nm high-reflection (HR) coatings, the laser damages induced by the shorter 532 nm wavelength exhibit very different damage characteristics and mechanisms. In this Letter, the initiators that induce damages under a single- and multi-shot laser at 532 nm are identified. The influences of the shot numbers and laser fluence on the damage morphologies and damage depth are investigated specifically to further discuss the fatigue effect caused by cumulative laser irradiations.

The HR coatings were deposited on BK7 substrates with a diameter of 50 mm via e-beam evaporation. The starting materials were hafnium and silica. All coatings runs used the same deposition technology and were in the same coating chamber. The coating stack was [BK7/6L(HL)^10H4L/Air], where H denoted the quarter-wavelength optical thickness of HfO_2, and L denoted the quarter-wavelength optical thickness of SiO_2. The total thickness of the film was about 2.6 μm. The reflectance of the HR coatings at 532 nm was more than 99.5% at an angle of incidence of 0°.

The laser damage test apparatus used in this study and error analysis were introduced in Ref. [12]. A 10 ns Nd:YAG laser operating at 532 nm in single longitudinal mode with up to a 5 Hz repetition rate was used. In our tests, the $1/e^2$ spot diameters on the x and y-axis measured via the knife-edge method were 282 and 404 μm. Twenty sites for each energy density were tested and the fraction of sites damaged was recorded. The site spacing was 1.5 mm, which was about five times greater than that of the laser spot diameter.

The damage morphologies were observed by a Leica microscope. A Zeiss dual beam microscope that combined the functions of a scanning electron microscope (SEM) and a focused ion beam (FIB) was used to obtain the

details of the damage morphologies and central structures. An atomic force microscopy (AFM) and a step profiler with a 2 μm pinhead radius were also employed in mapping the damage depth.

S-on-1 damage probability curves, with *S* ranging from 1 to 1000, are shown in Fig. 1(a). They clearly show an increase in the damage probability and a clear decrease in the damage threshold with an increasing number of shots[13,14]. Each of the shown curves is acquired using an independent measurement. Figures 1(b) and 1(c) present the evolution of laser induced damage threshold (LIDT) and the 100% damage probability threshold, respectively, versus the shot number derived from Fig. 1(a) by linear fit.

The decrease of LIDT and the 100% damage probability threshold with the increase of shot numbers is apparent, distinctly revealing the so-called fatigue effect. More tests are carried out to get the stable values of the LIDT and the 100% damage probability threshold. After 300 shots, the LIDT tends to a stable value, whereas the 100% damage probability threshold reached the saturation point after 3000 shots. The stable values of the LIDT and the 100% damage probability threshold are 6.4 and 11.2 J/cm^2, respectively. Comparing with the LIDT, the 100% damage probability threshold of multiple-pulse irradiations decreases more notably and needs more shots to incline to stabilization.

More importantly, it can be found from Fig. 1 that the increase in the damage probabilities are much more pronounced at a high laser fluence than those at a low laser fluence for fixed shot numbers. Meanwhile, the 100% damage probability threshold's decrease is much more pronounced than those of the LIDTs with the increase of the shot numbers. The results may suggest that the cumulative effects are larger at a high fluence than those at a low fluence.

Morphology observations enable the precise viewing of the damage characteristics and the identification of the damage initiators of the coatings. The damage morphology may be influenced by the laser fluence, shot numbers, and defect types and densities in the irradiated area at the same time. Figure 2 shows three different damage sites at a laser fluence of 19.7 J/cm^2 in the one-on-one case tested by optical microscopy. It can be seen from Fig. 2 that the typical damage morphologies are pits surrounded by large areas of plasma scalding, and the morphologies are different among the three damage sites. In order to investigate the reasons for this difference, we use the SEM to map the detailed information of the three damage morphologies. Figure 3 shows the high-resolution SEM image of Fig. 2. We can see that all the damage morphologies have micrometer-scale molten pits in the damage site as shown in Fig. 3, illustrating that the damage initiators are the submicron defects. Additionally, the three damage morphologies are different because of the nonuniform defect distributions. The higher the defect density in the laser-irradiated region, the more serious the damage is, as shown in Fig. 3(c), where the damage is much more serious than in Figs. 3(a) or 3(b). It can be seen from Fig. 3(c) that

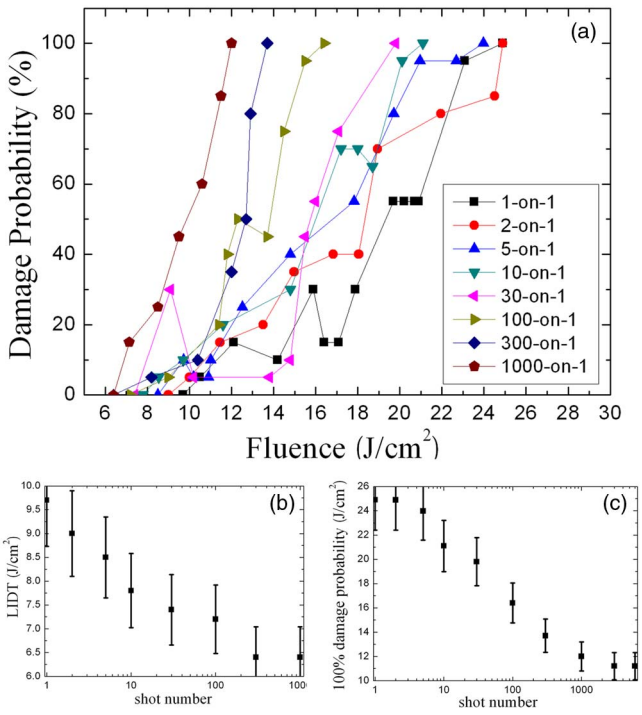

Fig. 1. (a) *S*-on-1 probability curves of 532 nm HR coatings, (b) and (c) are the evolution of LIDT and 100% damage probability threshold versus shot number.

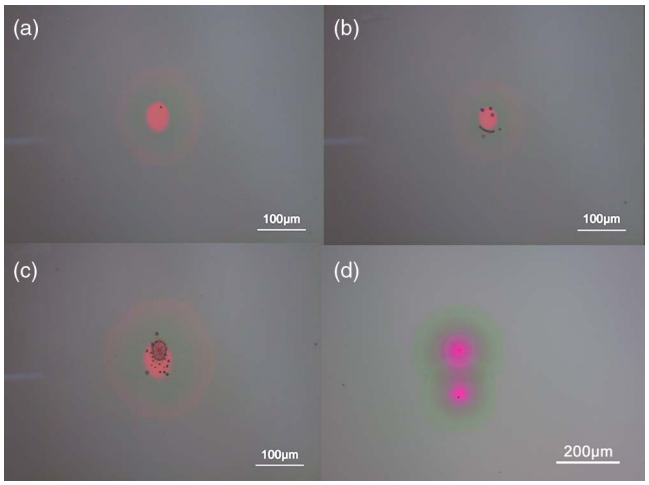

Fig. 2. Damage morphologies for (a)–(c) fluence of 19.7 J/cm^2 at 532 nm, (d) 86.7 J/cm^2 at 1064 nm in one-on-one mode tested by optical microscopy.

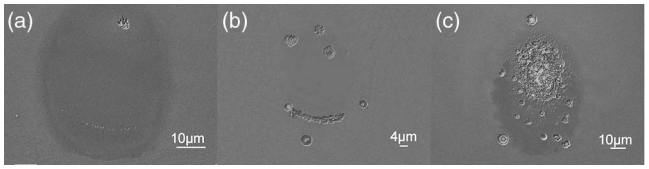

Fig. 3. SEM micrographs of the damage sites shown in Figs. 2(a)–2(c).

the damage pits form a region with a lateral size of about dozens of microns, going with the appearance of the delamination within this region. Except for pits, the other part of the damage is a plasma scald. The peripheral scald and the central severe scald (the pink area) behave as surface discoloration under the microscope. But the discoloration of peripheral plasma scald is light, as indicated in Fig. 4, which shows the SEM image of the damage site shown in Fig. 2(a) as an example. For laser damages in multilayer thin films at 1064 nm, the central severe plasma scalds are mostly pit-centered[12,15], as shown in Fig. 2(d), which shows a damage site in the one-on-one mode of irradiated laser fluence 86.7 J/cm^2 at 1064 nm. However, for 532 nm laser damages, we find the shapes and sizes of the central plasma scalds are independent of the defect position and density, as shown in Figs. 2(a)–2(c). Besides, the central plasma scalds are exactly at the center of the irradiated sites and the sizes of the scalds are basically the same. We think that the sizes of central plasma scalds are related to the high-intensity region of the Gaussian laser beam.

In order to confirm the above ideas and investigate the relationship between the laser fluence and the size of central scald, the damage morphologies at different laser fluences are studied. Figure 5 shows the typical sites at laser fluences of 10.5, 12.1, 19.7, and 24.9 J/cm^2 in the one-on-one case. We can see from Fig. 5 that the size of the plasma scald increases with the laser fluence, which agrees well with the above inference.

To reveal the damage initiators, depth information is tested using AFM and a step profiler. The results tested by the step profiler illustrate that the edges of the peripheral plasma scalds are several nanometers high compared with the undamaged film surface. In our samples, the maximum depths of the central scalds range from dozens of nanometers to more than 100 nm, which are much less than the thickness of the SiO_2 outer layer. Figure 6 is the depth information of the damage site shown in Fig. 2(a). The probe of the step profiler moves along the white line shown in the inset of Fig. 6.

Figure 7 illustrates the depth information and SEM micrograph of the damage pit shown in Fig. 5(a). Because the thermal effect for the 532 nm laser damage is not prominent like the 1064 nm laser damage[12], the bottom of damage pits for 532 nm are thus not smooth as those of 1064 nm. The test result of AFM shows that there is a one-to-one correspondence between the depths of the pit bottoms and the depths of the first four layers, which are 377, 445, 539, and 607 nm, respectively. Additionally, we find that the depths of the damage initiators have a close relationship to the electric intensity distribution in the multilayer thin films[16]. For our film, the second, fourth, and sixth interfaces have the three weakest squared electric fields, which are 1.02, 0.54, and 0.29. It can be seen from Fig. 7 that the damage precursor of this

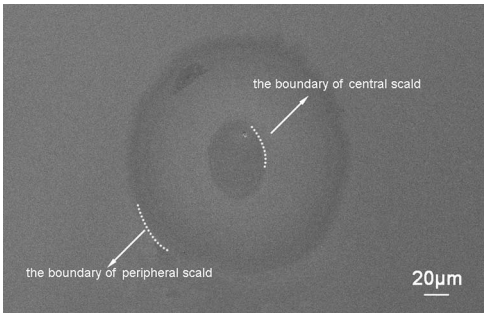

Fig. 4. SEM micrograph of the damage site shown in Fig. 2(a).

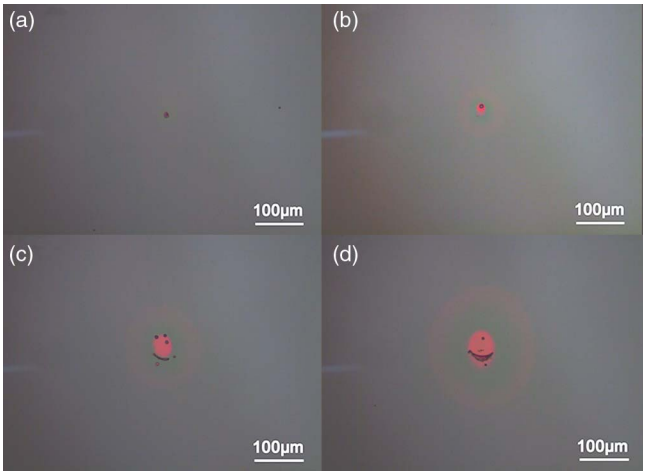

Fig. 5. Damage morphologies for fluence of (a) 10.5, (b) 12.1, (c) 19.7, and (d) 24.9 J/cm^2 at shot number $N = 1$.

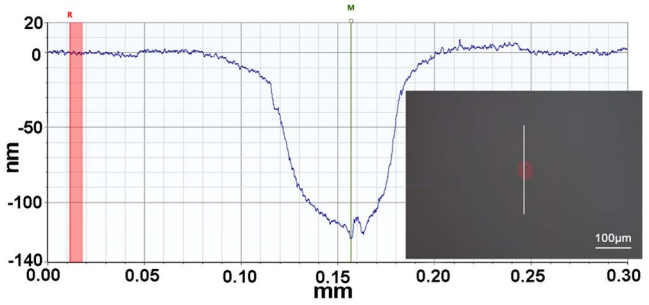

Fig. 6. Depth information of the plasma scald area for the damage site shown in Fig. 2(a). The probe of the step profiler moves along the white line.

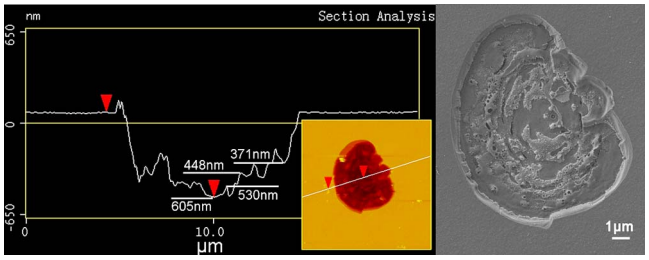

Fig. 7. AFM section analysis and SEM micrograph of damage at 10.5 J/cm^2 for $N = 1$.

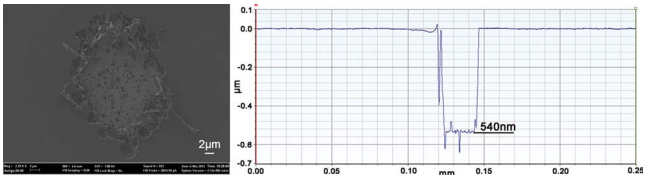

Fig. 8. Surface profiler of the damage sites at fluence 24.9 J/cm^2 for shot number $N = 1$.

damage site corresponds to the depth of the fourth interface.

The depth information of the much more serious damages is tested as well. Figure 8 is the result tested by the step profiler of the site damaged at a fluence of 24.9 J/cm^2 for shot number $N = 1$. It shows that the depth of the molten pits correspond to the fourth interface too, while the depth of delamination corresponds to the third interface. For single-pulse irradiation, the delamination more easily occurs when the laser fluence and defect density in the irradiated area are high simultaneously. The statistical results verify that the delaminations all occur at the third or first interface in our samples. Because the electric intensities at the first and third interfaces are zero, the possible cause of delamination is the weak binding force at the interface of SiO_2 deposited on HfO_2[17–19]. As we know, the silica layer is smooth, whereas the hafnia layer is relatively rough because of its columnar structure. Therefore, there will be more interfacial voids at the interface of SiO_2 deposited on HfO_2, as shown in Fig. 9 (the inset is a close zoom of interfaces 2 to 6). Thus, to reduce the occurrence of pits and delamination, we should improve the design to reduce the electric intensity at the interface and ameliorate the deposition technology to reduce the defect density and enhance the binding force at the interfaces.

We do not find that there are damage sites that start at the sixth interface under single-pulse irradiation.

In order to explore the fatigue effect of the multiple-pulse irradiations and the damage mechanism, the

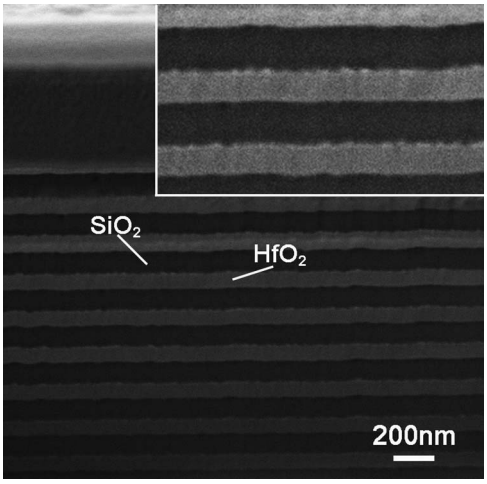

Fig. 9. The FIB micrograph of the 532 nm HR coatings.

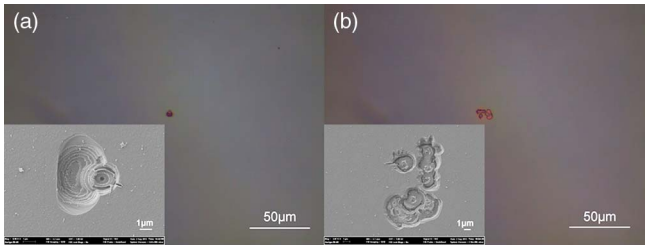

Fig. 10. Damage morphologies for (a) 18 J/cm^2, $N = 10$ and (b) 14.8 J/cm^2, $N = 30$, tested by optical microscopy and SEM.

damage morphologies and damage depth are studied in detail. Figure 10(a) shows a damage site at a fluence of 18 J/cm^2 for pulse number $N = 10$. The damage occurs at the ninth pulse. Figure 10(b) is a damage site with an irradiated laser fluence of 14.8 J/cm^2, which was damaged at the twenty-ninth pulse. Obviously, the damages caused by cumulative laser-induced material modifications are very different from the typical morphologies of single-pulse irradiation. From Fig. 10, we can see that the damage sites induced by multi-pulse irradiations exhibit only pits without an area of plasma scald around them, and the morphologies are almost the same at different fluences and pulse numbers. As for the reason for the damages with plasma scalds under single-pulse irradiation and the damages without plasma scalds at multiple-pulse irradiations, multiple-pulse laser-induced material modifications or new defect formations may be responsible for the phenomenon. Chambonneau *et al.* have shown the impact of the laser wavelength and laser fluence on the initiation of plasma scalds[20]. However, the plasma scalding exhibits different behaviors under single- and multi-pulse irradiations even at the same laser wavelength and fluence, and much more work needs to be done to clarify the reason for this phenomenon.

To confirm the reason for this phenomenon, the depth information for damages induced by multiple pulses is tested. Figure 11 reveals the depth information of the damage site shown in Fig. 10(a). The AFM result shows that the depth of the damage pit is about 760 nm, corresponding to the sixth interface of the coatings. The majority of the damage sites induced by

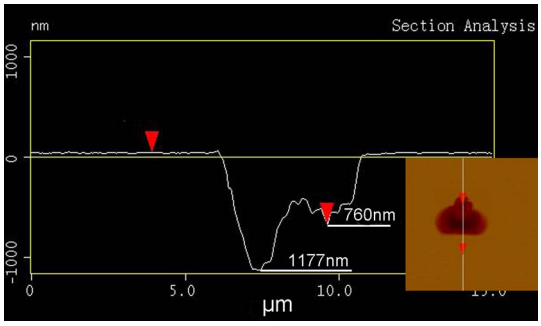

Fig. 11. The AFM section analysis of the damage site shown in Fig. 10(a).

cumulative multiple-pulse irradiations start at the sixth interface, while only a small part of the damage sites correspond to the fourth interface. The deeper damage depth for multiple-pulse irradiations clarifies that the damages for single- and multiple-pulse irradiations are induced by different kinds of defects, and further confirms the fatigue effect. For multiple-pulse irradiations, under the effect of the early laser pulses, the defects at the interface of relatively low electric intensity may make reversible or irreversible changes[21,22]. Within the relaxation time of reversible changes, if there are subsequent pulses irradiated, the damage occurs at last. The more pulses are irradiated, the more changes will take place, resulting in the increase of the damage probability and the decrease of LIDT with increasing pulse numbers. The damage site shown in Fig. 10(a) grows after the last laser pulse, resulting in the deeper mechanical delamination at the left of the damage pit. Figure 11 illustrates that the depth of this delamination corresponds to the eleventh interface, which is the same as the phenomenon of single-pulse irradiation. Because of the weak binding force, the delamination occurs at the interface of SiO_2 deposited on HfO_2.

In conclusion, the damage characteristics and damage mechanism for 532 nm HR coatings under single- and multiple-pulse irradiations are discussed. Single-pulse damages are attributed to the defects and the electric intensity distribution in the multilayer thin films. Other than the 1064 nm laser damage, the plasma scalds of the 532 nm laser damages are not pits-centered under normal incidence, but all at the center of the irradiated sites. The plasma scalding has no relation to the defect density and position, but increased with the laser fluence. For multiple-pulse irradiations, the damage morphology and depth information both clarify the fatigue effect further. The majority of the damage sites shows deeper precursors than those of single-shot irradiation. The cumulative laser-induced damages behave as pits without plasma scalding around them, which is unaffected by the laser fluence and shot numbers.

However, much more work needs to be done to clarify the formation of the plasma scalding and its difference among different wavelengths and shot numbers.

This work was supported by the National Natural Science Foundation of China under Grant Nos. 11104293 and 61308021.

References

1. L. Jensen, M. Mende, S. Schrameyer, M. Jupé, and D. Ristau, Opt. Lett. **37**, 4329 (2012).
2. J. Liu, W. Zhang, H. Cui, J. Sun, H. Li, K. Yi, and M. Zhu, Chin. Opt. Lett. **12**, 083101 (2014).
3. A. E. Chmel, Mater. Sci. Eng. B **49**, 175 (1997).
4. K. R. Manes, H. G. Ahlstrom, R. A. Haas, and J. F. Holzrichter, J. Opt. Soc. Am. **67**, 717 (1977).
5. L. Gallais, J. Y. Natoli, and C. Amra, Opt. Express **10**, 1465 (2002).
6. A. E. Chmel, Glass Phys. Chem. **26**, 49 (2000).
7. F. R. Wagner, A. Hildenbrand, H. Akhouayri, C. Gouldieff, L. Gallais, M. Commandre, and J. Y. Natoli, Opt. Eng. **51**, 121806 (2012).
8. J. Capoulade, L. Gallais, J. Y. Natoli, and M. Commandre, Appl. Opt. **47**, 5272 (2008).
9. X. F. Liu, D. W. Li, Y. A. Zhao, and X. Li, Appl. Opt. **49**, 1774 (2010).
10. K. H. Guenther, Appl. Opt. **20**, 1034 (1981).
11. H. Krol, L. Gallais, C. Grezes-Besset, J. Y. Natoli, and M. Commandre, Opt. Commun. **256**, 184 (2005).
12. W. W. Liu, C. Y. Wei, J. B. Wu, Z. K. Yu, H. Cui, K. Yi, and J. D. Shao, Opt. Express **21**, 22476 (2013).
13. F. R. Wagner, C. Gouldieff, and J. Y. Natoli, Opt. Lett. **38**, 1869 (2013).
14. J. Y. Natoli, B. Bertussi, and M. Commandre, Opt. Lett. **30**, 1315 (2005).
15. X. F. Liu, Y. A. Zhao, D. W. Li, G. H. Hu, Y. Q. Gao, Z. X. Fan, and J. D. Shao, Appl. Opt. **50**, 4226 (2011).
16. Y. G. Shan, H. B. He, Y. Wang, X. Li, D. W. Li, and Y. A. Zhao, Opt. Commun. **284**, 625 (2011).
17. F. Kong, Y. Jin, S. Liu, S. Chen, H. Guan, K. He, Y. Du, and H. He, Chin. Opt. Lett. **11**, 102302 (2013).
18. C. J. Stolz, F. Y. Genin, M. R. Kozlowski, and Z. L. Wu, Inertial Confinement Fusion Quarterly Report **9**, 151 (1999).
19. Z. Yu, H. He, X. Li, H. Qi, and W. Liu, Chin. Opt. Lett. **11**, 073101 (2013).
20. M. Chambonneau, R. Diaz, P. Grua, J. L. Rullier, G. Duchateau, J. Y. Natoli, and L. Lamaignere, Appl. Phys. Lett. **104**, 021121 (2014).
21. L. A. Emmert, M. Mero, and W. Rudolph, J. Appl. Phys. **108**, 043523 (2010).
22. M. Mero, J. Liu, and W. Rudolph, Phys. Rev. B **71**, 115109 (2005).